ADVANCED MATERIALS

Supporting Information

for *Adv. Mater.*, DOI: 10.1002/adma.201706368

Metasurface Enabled Wide-Angle Fourier Lens

Wenwei Liu, Zhancheng Li, Hua Cheng, Chengchun Tang, Junjie Li, Shuang Zhang, Shuqi Chen,* and Jianguo Tian*

Supporting Information

Title: Metasurface Enabled Wide-Angle Fourier Lens

Wenwei Liu, Zhancheng Li, Hua Cheng, Chengchun Tang, Junjie Li, Shuang Zhang, Shuqi Chen*, and Jianguo Tian*

S1. Design methods and supplementary experimental results

Light path differs for a Fourier lens and an imaging lens. As shown in Figure S1. For a Fourier lens, the foci offset is $l_1 = f \sin\theta$, which is proportion to the Fourier component of the wavefront.[7] However, for an imaging lens, light passes optical center of the lens without change of propagating direction, resulting in a foci offset of $l_2 = f \tan\theta$. When the lens is thin enough meeting the paraxial condition, l_1 approximately equals to l_2, and the lens is simultaneously a Fourier lens and an imaging lens.

Figure S2 shows the photographs of the focal plane with different incident wavelengths and angles. With normal incidence, the focal lines are aligned in the vertical direction, while for oblique incidence the focal lines show different offset. This can be attributed to the dispersive characteristic of the metalens. Achromatic focusing is often significant in many applications,[25–27] and this is a future challenge for the Fourier metalens. The vertical cut in the focal plane for 1100 to 1700 nm incidence is shown in Figure S3. It can be seen that all the results exhibit a FWHM of ~λ. Although our results do not break the diffraction limit, the FWHM of the Fourier metalens is close to the metalens designed as an imaging one.[28]

With multi−wavelength incidence (1100, 1300, 1500, 1700 nm), the focal line shows a focus depth of about 44 μm (Figure S4a). Although only four wavelengths are applied, the

four foci link with each other, and an ultra−wide focusing is obtained. This may benefit microfabrication technologies. With oblique incidence, the ultra−wide foci slightly separate.

We computed the Modulation transfer function (MTF) with the measured vertical cut of the focusing lines in Figure S5. The MTFs for 0−60° incidence are near to each other, and decrease to their minimum at 600 cycles/mm. The diffraction limited spatial frequency can be calculated through f_c = 2NA/λ.= 1104 cycles/mm, which accords with the FWHM of the vertical cut in Figure S3. The experimental setups are illustrated in Figure S6. In the measurement of focusing efficiency, the camera is replaced with a power meter integrated with an iris. The incident energy is measured by replacing the metalens with a gold window with the same size as the metalens.

S2. Simulated amplitude, phase, and intensity distribution of the metalens

The designed phase profile is described by **Error! Objects cannot be created from editing field codes.**, where $\varphi(0, \theta)$ is the phase at zero point under an oblique incident angle θ. The necessity of computing the phase difference can be seen in Figure S7 and S8. The absolute phase value varies for different incident angles, especially when the incident angle exceeds 30°. Fortunately, it is the relative phase that decides the wavefront. This is a basic constraint condition during simulations. As shown in Figure S9, we achieved a near angle−dispersion−free phase profile with the eight DWs. To statistically quantify the fluctuation of the phase for different incident angles, we calculate the standard deviation (STD) of the phase factor $s_i = e^{-i(\varphi_i - \varphi_1)}$ with $STD = \sqrt{\frac{1}{N}\sum_{i=1}^{N}\left|s_i - \bar{s}\right|^2}$, as shown in Figure S12. The waveguide mode for broadband behavior is demonstrated in Figure S13.

Supplementary figures

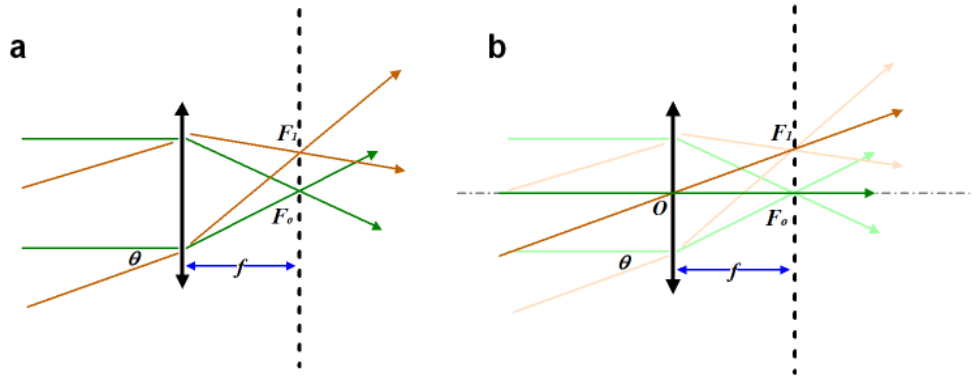

Figure S1. Schematic of the light path for metalenses. (a) Light path for a Fourier metalens with normal incident foci F_o and oblique incident foci F_1. (b) Light path for an imaging metalens with normal incident foci F_o and oblique incident foci F_1.

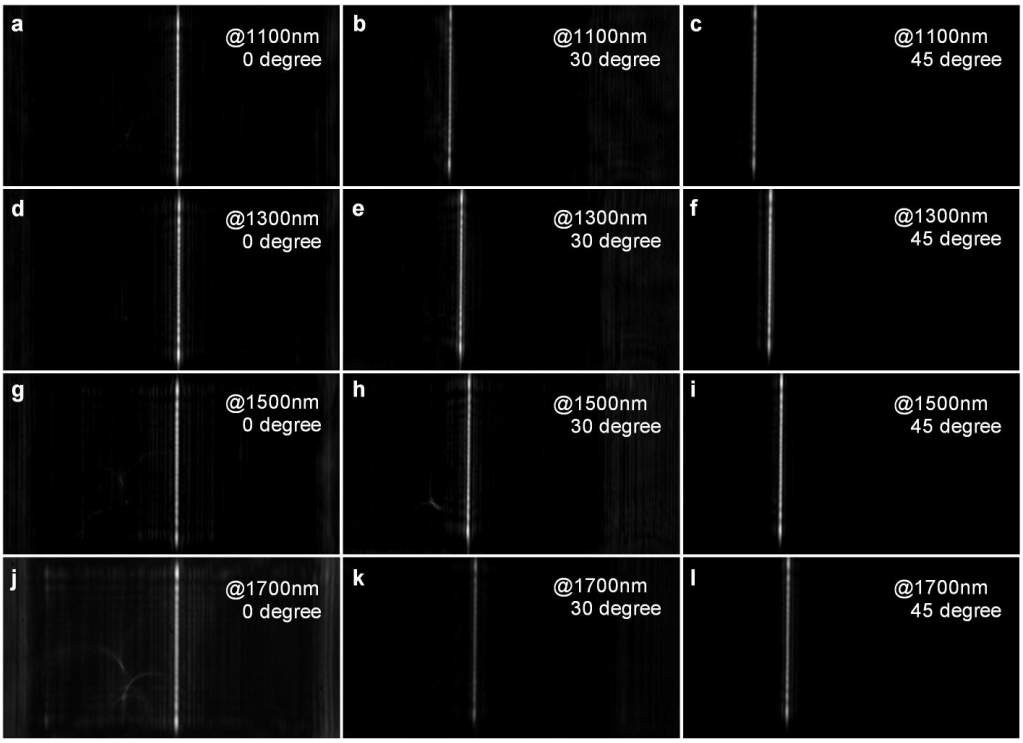

Figure S2. Photographs of the focal plane taken by the InGaAs camera with different incident wavelengths and angles. The incident wavelength for (a) to (l) is 1100−1700 nm, the incident angle is 0−45°, as marked in each figures.

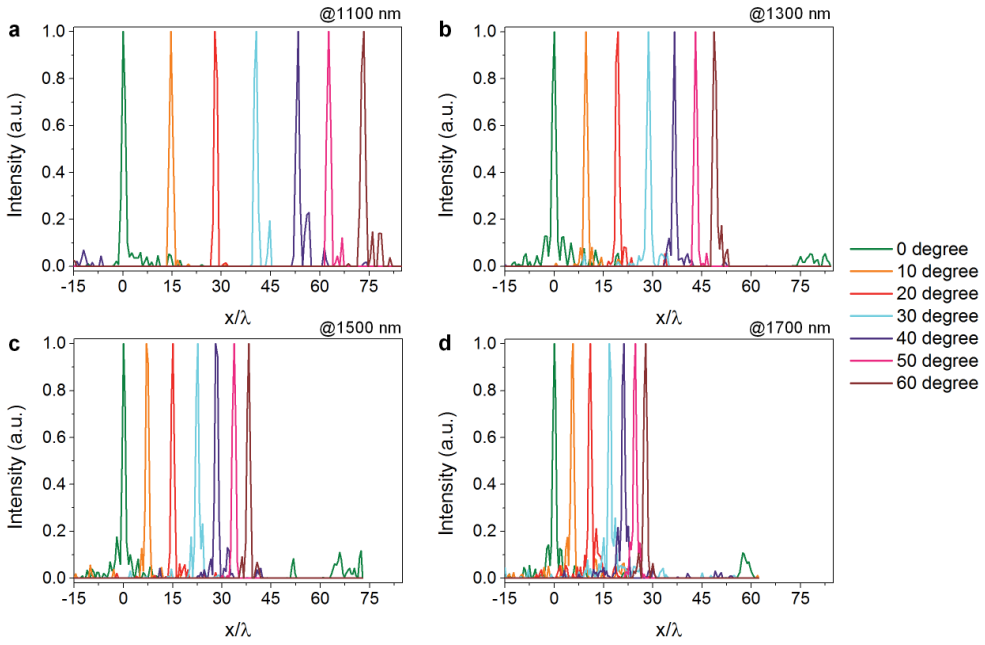

Figure S3. Measured focusing vertical cut for different incident wavelengths and angles. The incident wavelength is (a) 1100 nm, (b) 1300 nm, (c) 1500 nm, (d) 1700 nm.

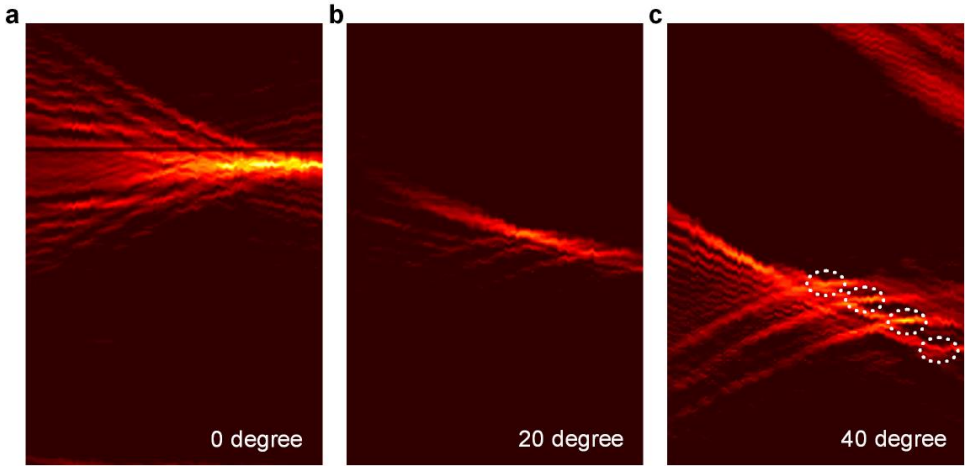

Figure S4. Measured focusing intensity with multi−wavelength incidence of 1100, 1300, 1500, and 1700 nm. The incident angle is (a) 0 degree, (b) 20 degree, (c) 40 degree. The dashed circles in (c) indicate separate foci under 40 degree incidence.

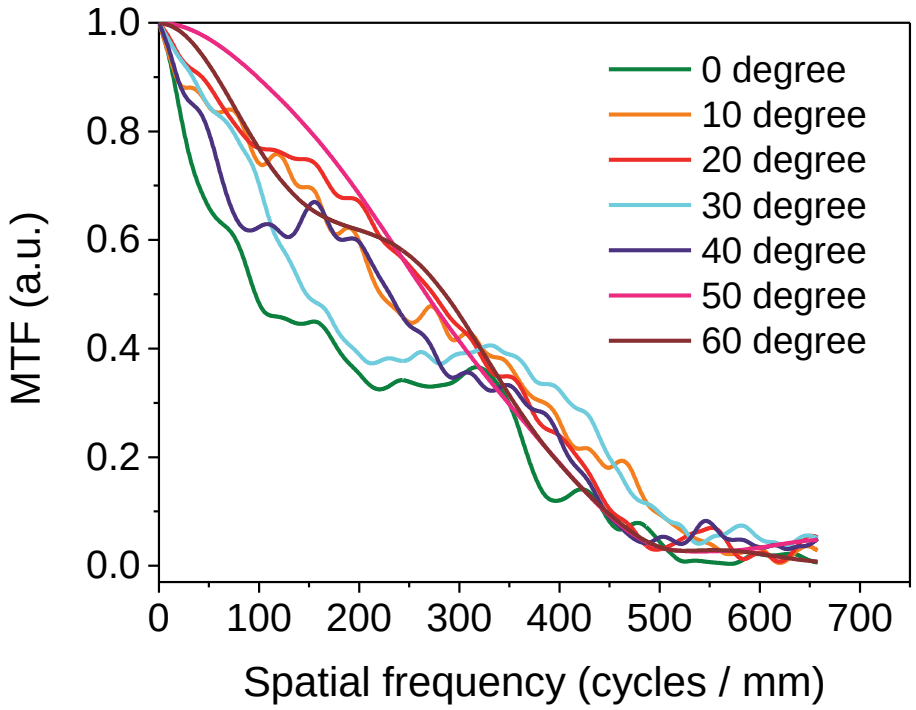

Figure S5. Modulation transfer function (MTF) computed through measured focusing vertical cut for different incident angles with 1500 nm incidence.

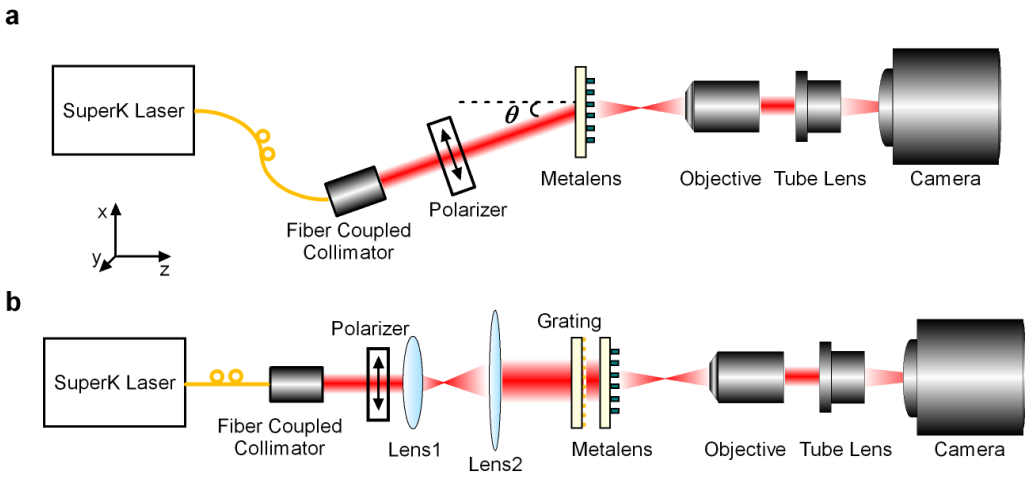

Figure S6 Measurement setup. (a) Schematic illustration of the measurement setup used for oblique incidence. The Fiber coupled collimator and polarizer are integrated on a rotational stage, and the objective, tube lens, and camera are integrated on an XYZ translation stage. (b) Schematic of Fourier transform of a grating. The combination of lenses are used to magnify the diameter of the laser beam.

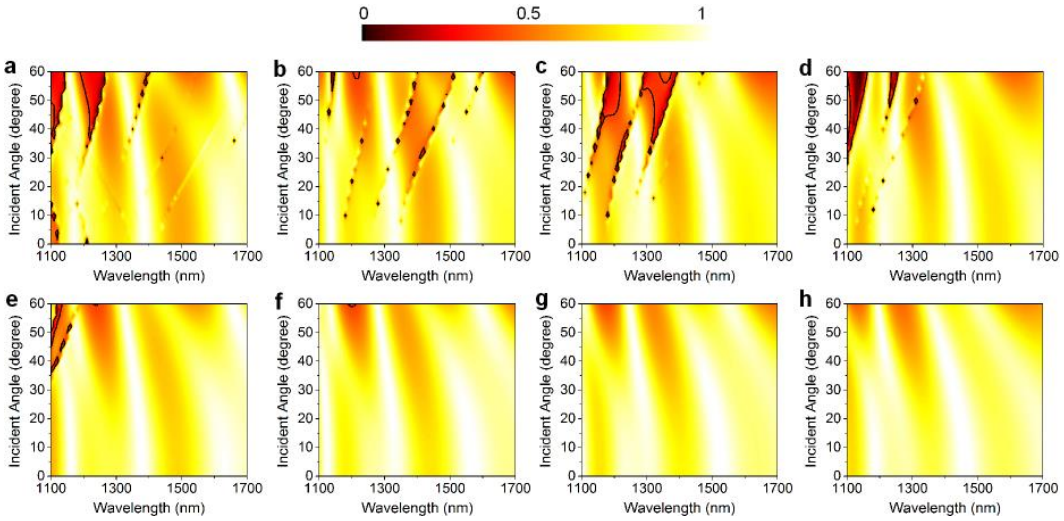

Figure S7. Simulated transmission as a function of incident wavelength and angles. (a)−(h) correspond to the chosen eight widths of DWs in Figure 2d in the main text. Black lines in each graph depict a contour height of 0.5.

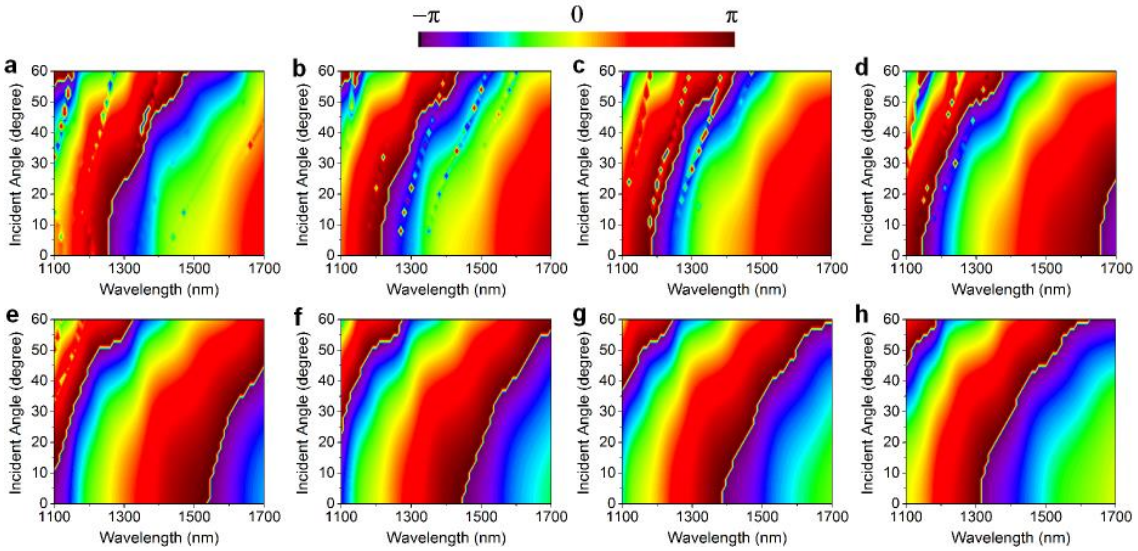

Figure S8. Simulated phase difference as a function of incident wavelength and angles. (a)−(h) correspond to the chosen eight widths of DWs in Figure 2d in the main text.

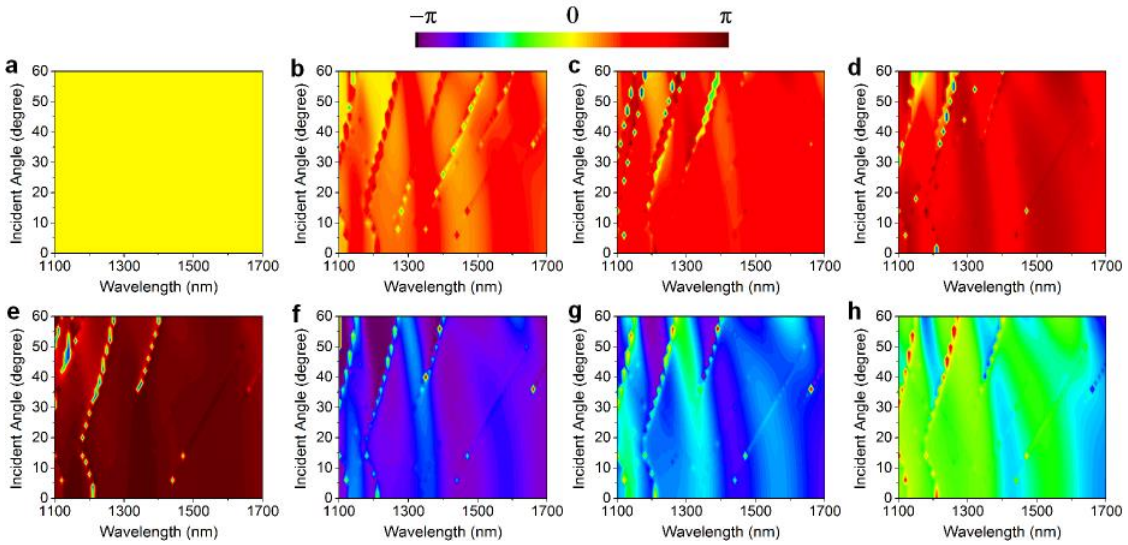

Figure S9. Simulated phase difference subtracting the phase of the first structure as a function of incident wavelength and angles. (a)−(h) correspond to the chosen eight widths of DWs in Figure 2d in the main text.

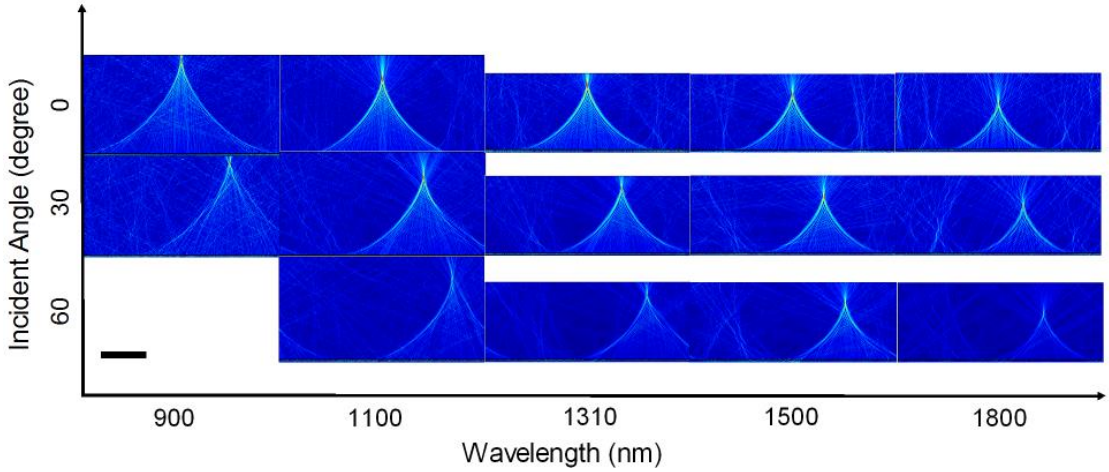

Figure S10. Simulated focusing profiles with different incident wavelengths and angles. Scale bar, 60 μm.

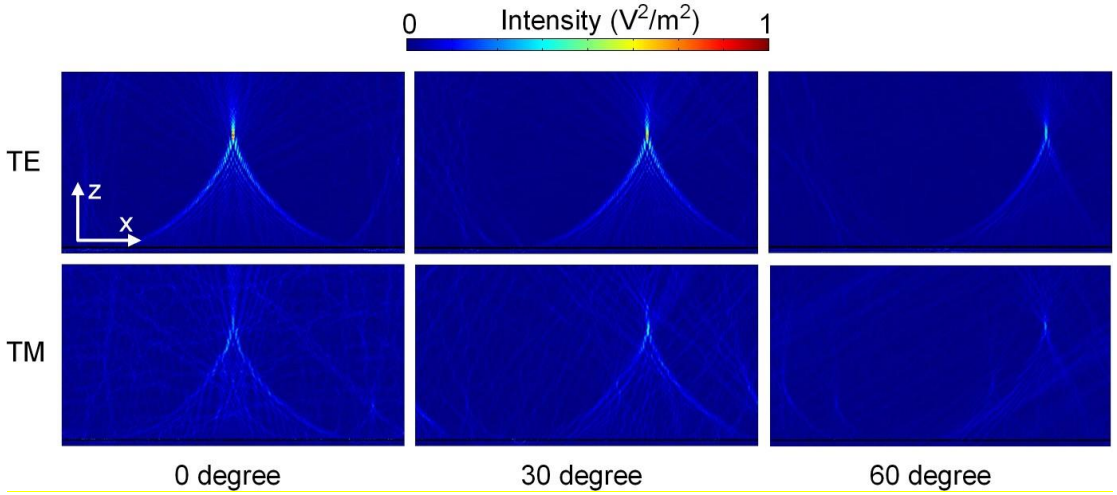

Figure S11. Simulated focusing profiles under TE and TM incidence of 1550 nm. The incident angles are 0 degree, 30 degree, and 60 degree, respectively.

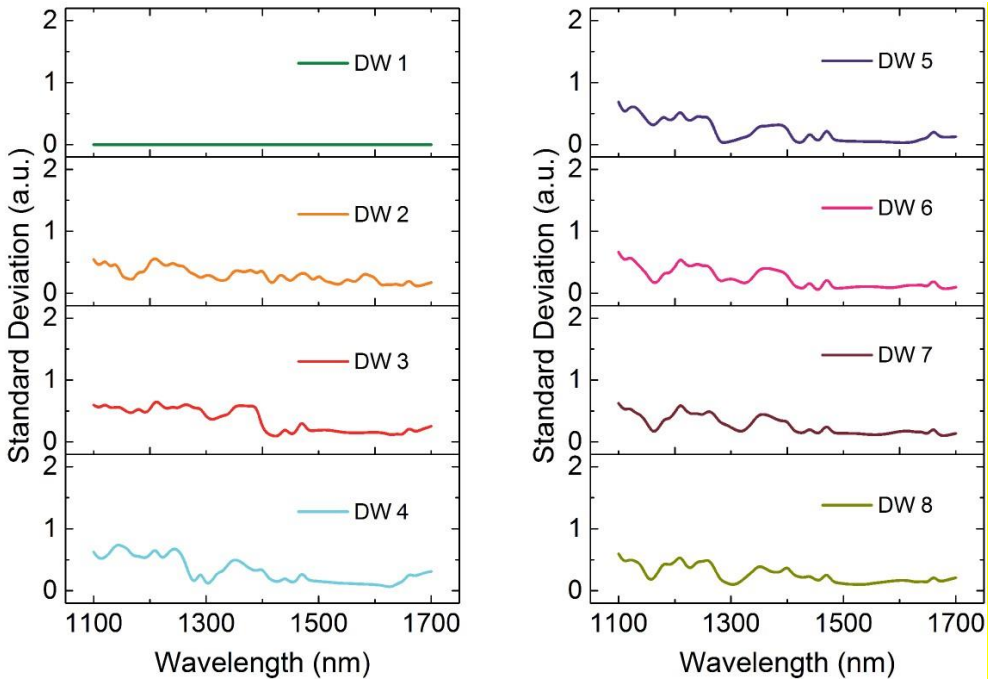

Figure S12. Calculated standard deviation of the phase factor of the phase-change based on Figure. S9.

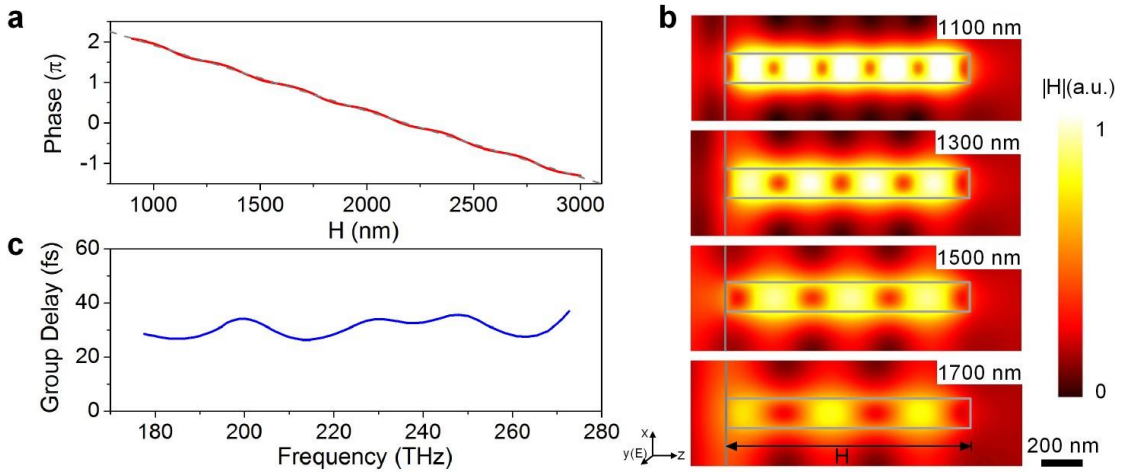

Figure S13 (a) Simulated phase of the DW 7 with varied height of the DW. The gray dashed line is the linear fit of the phase function. (b) Simulated waveguide mode of DW 7 with incident wavelength of 1100 nm, 1300 nm, 1500 nm, and 1700 nm respectively. (c) Calculated group delay of DW 7 over the working waveband.

Supplementary video legends

Movie S1. Fourier transform of a grating at a wavelength of 1100 nm. The movie shows the evolution of the filed intensity when moving the translation stage along the light−propagating direction.

(Movie S2, S3, S4 are recorded at wavelengths of 1300, 1500, 1700 nm, respectively.)

Movie S5 Spatial filtering with the Fourier metalens. The movie shows the appearance and disappearance of the diffraction order when moving the grating in the cross direction. The operating wavelength is 1300 nm.